Title:

CDK4/6 inhibition promotes senescent states with restricted secretory phenotype and reduced toxicity

Authors:

Boshi Wang[1], Simone Brandenburg[1], Alejandra Hernandez-Segura[1], Thijmen van Vliet[1], Elisabeth M. Jongbloed[2], Saskia M Wilting[2], Naoko Ohtani[3], Agnes Jager[2] and Marco Demaria[1]*

Affiliations:

[1]European Research Institute for the Biology of Ageing (ERIBA), University Medical Center Groningen (UMCG), 9713AV Groningen, The Netherlands

[2]Department of Medical Oncology, Erasmus MC Cancer Institute, Erasmus University Medical Center, 3015GD Rotterdam, The Netherlands

[3]Graduate School of Medicine, Osaka City University, 545-8585, Osaka, Japan

[*]Correspondence to: m.demaria@umcg.nl

Lead contact: m.demaria@umcg.nl

This PDF includes:

Main Text

Figures 1-5

Abstract

Cellular senescence is a state of stable growth arrest that acts as a tumor suppressive mechanism. Genotoxic agents exert their anti-cancer functions partly by inducing cancer cells into senescence. However, because of systemic administration and lack of specificity, treatment with genotoxic agents is associated with premature senescence of various non-cancerous cells. Therapy-induced normal senescent cells can have profound detrimental pro-tumorigenic and pro-disease functions via activation of a pro-inflammatory secretory phenotype (SASP). Alternative to genotoxic agents, inhibitors of cyclin-dependent kinases 4/6 (CDK4/6i) have recently proven to be potent anti-cancer interventions able to activate a poorly characterized senescence-like state. Here, we demonstrate that establishment of CDK4/6i-induced stable growth arrest is dependent on p53 transcriptional activity. We show that in human cells, mouse tissues and plasma of metastatic breast cancer patients the CDK4/6i-induced senescent program engages only a partial SASP enriched in p53-associated genes (PASP) but without pro-inflammatory and detrimental NF-κB-dependent factors (NASP). Because of the lack of a NASP, CDK4/6i-induced $p16^{+}$ senescent cells do not exert detrimental and pro-tumorigenic functions in culture and *in vivo*. Interestingly, short-term treatment of chemotherapy-induced senescent cells with CDK4/6i is sufficient to partially reduce an already established NASP and improve mouse healthspan via p53 activation and NF-κB repression. Our data suggest that short- and long-term treatment with CDK4/6i can modulate senescence-associated phenotypes and restrict the detrimental effects of senescent cells in cancer therapy.

Keywords

Cellular senescence; growth arrest; SASP; aging; CDK4/6 inhibitors; chemotherapy; side effects; chemotoxicity; abemaciclib; palbociclib; paclitaxel; doxorubicin

Introduction

Unrestrained proliferation is one of the common hallmarks of cancer cells, and a major target for anti-cancer interventions[1]. Genotoxic therapies, such as chemo and radiotherapy, cause high level of DNA damage in quickly proliferating cells often leading to cell death or states of stable cell cycle arrest[2]. A major advantage of genotoxic interventions is that they are not biased to specific molecular marks or cell types, and are effective against a broad range of tumor specimens. However, this lack of specificity is also the basis of several short- and long-term adverse reactions which arise from inflicting unrepairable DNA damage to actively proliferating normal cells.

A likely outcome of genotoxic agents is activation of cellular senescence – a state of stable growth arrest dependent on the upregulation of cyclin-dependent kinases (CDK) inhibitors p16 and p21, and associated to a complex Senescence-Associated Secretory Phenotype (SASP)[3]. Senescence induction acts as a potent tumor suppressive mechanism by restraining cancer cell proliferation and activating tumor immunosurveillance[4]. However, increasing evidence suggests that therapy-induced normal cells promote chronic inflammation and several short- and long-term adverse effects, including fatigue, myelosuppression, cardiomyopathy, bone loss, cancer progression and relapse, and that their genetic and pharmacological removal is sufficient to improve healthspan[5–8]. These senescence-associated detrimental effects are mainly mediated by pro-inflammatory SASP cytokines and chemokines, which are normally elevated in cancer patients suffering from a variety of adverse reactions to cancer therapies[9,10]. Major regulator of pro-inflammatory SASP genes is NF-κB, a transcription factor mediating the response to persistent DNA damage[11,12]. Senescent states activated by direct p16 or p53 overexpression do not show signs of DNA damage and activate a less inflammatory SASP[13–15]. Interestingly, p53 overexpression can also counteract NF-κB activity and reduce pro-inflammatory SASP in DNA damage-induced senescence[15–17]. In contrast to DNA damaging agents, a novel class of anti-cancer drugs potently interferes with cell cycle progression by inhibiting specific cyclin-dependent kinases (CDKs). Palbociclib (PD033291) and abemaciclib (LY2835219) are selective CDK4/6 inhibitors (CDK4/6i) approved by the U.S. FDA to treat hormone-sensitive and HER2 negative advanced breast cancer patients. Addition of a CDK4/6 inhibitor to hormonal treatment showed to improve progression free survival in large metastasized breast cancer patient cohorts[18,19] and under investigation as first line treatment for lung cancer patients[20]. Short-term treatment with CDK4/6i induces a temporary and reversible growth arrest, but long-term treatment promotes a poorly characterized state of cellular senescence[21,22]. Here, we set to study the mechanisms by which exposure to pharmacological CDK4/6i would cause normal and non-cancerous cells to enter senescence, the secretory phenotype of CDK4/6i-induced senescent cells and their

toxicity *in vivo*. Moreover, we analyze the modulation of senescence-associated phenotypes by short-term treatment with abemaciclib.

Results

Long-term CDK4/6i treatment induces cellular senescence in primary cells and mice

In accordance with previous studies[23], prolonged treatment of human primary fibroblasts (BJ) with abemaciclib was associated to a progressive loss of RB phosphorylation (Extended data Fig. 1a), down-regulation of *E2F2* (Extended data Fig. 1b) and increased *p16* gene expression (Extended data Fig. 1c). Reduced population doubling (Extended data Fig. 1d) and EdU incorporation (Fig. 1a) at the end of treatment demonstrated the efficacy of abemaciclib to induce cell cycle arrest. A similar proliferative arrest was observed in human primary fibroblasts WI38 treated with abemaciclib or palbociclib (Extended data Fig. 1e). Importantly, drug withdrawal was not sufficient to restore proliferation of CDK4/6i-treated cells (Fig. 1a,b and Extended data Fig. 1f,g), particularly after an 8-day treatment (Extended data Fig. 1h,i). CDK4/6i-treated cells assumed a flattened and enlarged morphology (Extended data Fig. 1j), activated the Senescence Associated-β-galactosidase (SA-β-gal) (Fig. 1c and Extended data Fig. 1k), and maintained high level of the endogenous CDK4/6i p16 (Extended data Fig. 1l), all features that can also be observed in cells treated with other anti-cancer and senescence-inducing agents such as the genotoxic drug doxorubicin[6]. RNA-sequencing analysis of cells 8 days post-treatment revealed that a great number of differentially expressed genes were shared between abemaciclib- and doxorubicin-treated cells (Fig. 1d). Down-regulation of cell cycle genes (Fig. 1e), up-regulation of lysosomal-associated pathways (Extended data Table 1) and activation of a 'core' transcriptional signature of senescence[24] (Fig. 1f) were observed in both abemaciclib- and doxorubicin-treated cells. To determine whether induction of cellular senescence happens *in vivo*, we exposed mice to a clinically-relevant and tumor suppressive dose of abemaciclib. At first, the anti-neoplastic effects of this dose (50 mg/kg/day of abemaciclib for 7 consecutive days) was validated in our laboratory using a model of breast cancer (Extended data Fig. 2a-c). Then, we treated cancer-free p16-3MR mice, which harbor a Renilla Luciferase (RL) reporter gene driven by the p16 promoter[25], with abemaciclib or doxorubicin. Abemaciclib- and doxorubicin-treated mice showed a similar enhanced bioluminescent signal (Fig. 1g,h), and comparable induction of p16 and SA-β-gal in kidneys (Fig. 1i,j and Extended data Fig. 2d). Together, these data suggest that prolonged treatment with CDK4/6i triggers a senescence response in human cells in cell culture and in mice *in vivo*.

CDK4/6i-induced senescence depends on p53

Despite p16 level being increased during CDK4/6i treatment (Extended data Fig. 1c) and maintained after drug withdrawal (Extended data Fig. 1l), loss-of-function models indicated that p16 was largely dispensable for activation of an irreversible growth arrest (Extended data Fig. 3a,b). Interestingly, RNA-sequencing data suggested that abemaciclib-treated BJ cells differentially expressed several p53 transcriptional targets related to cell cycle[26,27] at both 1 and 8 days post-treatment (Extended data Fig. 3c). To evaluate whether p53 was essential to orchestrate the irreversible cell cycle arrest in response to CDK4/6i, we analyzed various models with impaired p53 expression. BJ cells transduced with a genetic suppressor element (GSE) against p53[28] or with shRNA lentiviral particles (Extended data Fig. 3d) assumed enlarged morphology and activated a temporary arrest during abemaciclib or palbociclib treatment, comparable to what observed in WT cells (Extended data Fig. 1e,j and Fig. 3e,f). However, in the absence of p53 cells were able to restore proliferation after drug removal, as measured by colony-formation assays and EdU incorporation (Fig. 2a,b and Extended data Fig. 3g). Similarly, Mouse Dermal Fibroblasts (MDFs) derived from p53 knock-out mice and wild-type Mouse Embryonic Fibroblasts (MEFs) with inactive p53 also failed to enter irreversible growth arrest upon exposure to abemaciclib or palbociclib (Fig. 2c,d and Extended data Fig. 3h). The bypass of irreversible growth arrest in p53-deficient BJ cells was associated to a failure in modulating the expression of several p53 transcriptional targets related to cell cycle upon treatment with abemaciclib (Fig. 2e). BJ cells with stable expression of a luciferase reporter construct (p53LUC) confirmed gradual activation of p53 transcriptional activity upon exposure to abemaciclib, similar to what was observed in cells treated with the Mdm2 inhibitor nutlin-3a (Fig. 2f). Moreover, ChIP analyses revealed that abemaciclib enhanced p53 binding to the promoter regions of its target genes *CDKN1A (p21)*, *MDM2* and *GADD45A*, similar to what was observed upon exposure to nutlin-3a (Fig. 2g). To validate the dependence of CDK4/6-induced irreversible growth arrest on p53 transcriptional activity, we exposed BJ cells and p16-3MR mice to pifithrin-α (PFT-α), a reversible inhibitor of p53-dependent transcription[29]. The concomitant treatment abemaciclib/PFT-α allowed a substantial number of BJ cells to bypass the irreversible growth arrest (Fig. 2h). In mice, co-treatment abemaciclib/PFT-α prevented induction of whole-body luminescence and of p16 and p21 expression in tissues (Fig. 2i,j). Taken together, these data suggest that CDK4/6i induce a state of a senescence-associated permanent growth arrest dependent on p53 transcriptional activity.

Abemaciclib-induced senescent cells develop only a partial SASP

A characteristic senescence-associated feature is SASP activation[17]. RNA-sequencing data indicated that a vast majority of SASP genes were up-regulated in doxorubicin-induced senescent cells, while about half of these genes

were not differentially regulated or even down-regulated in abemaciclib-induced senescence (Fig. 3a). Importantly, a substantial number of SASP factors exclusively induced by doxorubicin treatment was predicted to be a direct target of the transcription factor NF-κB (Fig. 3a, in purple). NF-κB is considered the main regulator of the pro-inflammatory arm of the SASP[11], and a consequence of chronic DNA damage response (DDR) signaling[12]. Cells exposed to doxorubicin showed significant level of γ-H2AX staining but no signs of DNA damage were observed in cells exposed to CDK4/6i (Fig. 3b). As expected from the DNA damage levels, cells induced to senescence by abemaciclib or palbociclib did not enhance NF-κB activity, as measured by using a luminescent reporter system, whereas a strong upregulation was observed in cells induced to senescence by the genotoxic drugs doxorubicin or paclitaxel (Fig. 3c). qPCR experiments demonstrated that only genotoxic drugs, but not CDK4/6i, were able to induce several factors part of the NF-κB-Associated Secretory Phenotype (NASP) such as IL6, CXCL1, CCL5 and MMP1 in both human (Fig. 3d) and mouse cells (Extended data Fig. 4a). Cytokine array and ELISAs confirmed that NASP factors were up-regulated in the conditioned media (CM) of genotoxic stress-induced cells, but this induction was minimal or absent in CDK4/6i-treated cells (Fig. 3e and Extended data Fig. 4b). Among the SASP factors equally up-regulated in doxorubicin-induced and abemaciclib-induced senescence, a significant number was predicted to be p53 target (Fig. 3a, in green). To test whether the expression of these genes was regulated by p53, we exposed BJ cells to long-term treatment with the Mdm2 inhibitor nutlin-3a. As previously shown[14,15], prolonged treatment with nutlin-3a induced irreversible growth arrest (Extended data Fig. 4c) and enhanced transcription of the p53 target genes *p21*, *GADD45A* and *MDM2*, but these senescent cells fail to activate a NASP (Extended data Fig. 4d). Importantly, nutlin-3a-induced senescence was accompanied by up-regulation of the SASP genes and p53 targets *ISG15*, *IGFBP3*, *GDF15*, *TGFA* and *LIF*, supporting their dependence on p53 activity (Extended data Fig. 4d). qPCR and ELISA experiments confirmed the up-regulation of IGFBP3 and LIF, factors part of the p53-Associated Secretory Phenotype (PASP), in BJ cells induced to senescence by abemaciclib or palbociclib (Fig. 3f,g). Importantly, ChIP analysis showed that abemaciclib promoted a direct binding of p53 to the promoter region of the PASP factor IGFBP3 (Fig. 3h), and qPCR data showed that BJ cells lacking functional p53 failed to induce a PASP in response to abemaciclib or palbociclib (Extended data Fig. 4e). In alignment with cell culture measurements, doxorubicin treatment increased the concentration of CXCL1/KC in mouse plasma (Fig. 3i) and promoted expression of IL-6 and various other NASP factors in kidney and liver, while abemaciclib had no effects (Fig. 3j and Extended data Fig. 4f,g). In contrast, PASP factors *Isg15*, *Gdf15*, *Tgfa* and *Lif* were equally upregulated in the kidneys of mice exposed to doxorubicin or abemaciclib (Fig. 3k). Finally, to validate these findings in a clinically-relevant system, we measured the level

of NASP and PASP in the plasma of breast cancer patients treated either with genotoxic chemotherapy or CDK4/6i. Genotoxic therapy (paclitaxel) enhanced the plasma concentration of the NASP factors CXCL1 and CCL5 and the PASP factor IGFBP3, while treatment with palbociclib was associated with the sole up-regulation of the PASP factor IGFBP3 (Fig. 3l). These data suggest that treatment with CDK4/6i induces senescence with a PASP but without a NASP, and that PASP factors, but not NASP, are enhanced by palbociclib treatment in cancer patients.

Abemaciclib treatment exerts minimal toxicity

Senescent cells generated by genotoxic stress contributes to various toxicities, including tumor promotion and relapse, via secretion of various pro-inflammatory NASP factors[5–7]. Interestingly, exposure of MCF7 (breast cancer), A549 and HCC827 (lung cancer) cells to the CM of abemaciclib-induced senescent cells had a strongly reduced pro-proliferative effect in comparison to CM from doxorubicin-induced senescent cells (Extended data Fig. 5a,b). Similarly, co-injection of doxorubicin-induced or abemaciclib-induced senescent fibroblasts (BJ) and lung cancer cells (A549) into the flanks of *Foxn1*^{Nu} mice indicated that doxorubicin-treated, but not abemaciclib-treated, cells promoted tumor growth (Fig. 4a and Extended data Fig. 5c). Moreover, CM from doxorubicin-treated BJ cells promoted migration of MCF7 and A549 cells while no significant effect was observed in cells exposed to CM from abemaciclib-treated cells (Fig. 4b and Extended data Fig. 5d). To analyze toxicities *in vivo*, we exposed cancer-free mice to either CDK4/6i or genotoxic chemotherapy and measured various functional parameters. As previously shown, abemaciclib and doxorubicin induced comparable levels of senescence in cancer-free mice (Figure 1g-j). However, we observed that the protein level of HMGB1 was induced in kidneys of doxorubicin-treated but not abemaciclib-treated mice (Extended data Fig. 5e), implying that systemic treatment with CDK4/6i was not sufficient to promote a strong inflammatory response[30], in accordance to the absence of a NASP (Fig. 3g,h). During treatment, and up to 14 days post, doxorubicin-treated mice showed substantial weight loss, while abemaciclib-treated mice did not lose any weight (Fig. 4c). Blood cell counts in the abemaciclib-treated group did not differ when compared to control animals, while doxorubicin caused anemia, as measured by reduced number of red blood cells (Fig. 4d), and an overall slight decrease in the total number of leukocytes (Fig. 4e) with impaired proportion of B cells, granulocytes and macrophages (Fig. 4f). As previously shown[6], treatment with doxorubicin severely affected strength and physical activity, as measured by rotarod assay (Fig. 4g), grip strength (Fig. 4h) and hanging endurance (Fig. 4i) at both 7 and 14 days after treatment. In contrast, mice treated with abemaciclib did not show any apparent reduction of physical performances in comparison to vehicle-treated cohorts (Fig. 4g-i). To compare the effect on tumorigenesis of normal cells induced to senescence by CDK4/6i or genotoxic stress *in vivo*,

we treated mice with abemaciclib and doxorubicin and 7 days later transplanted the syngenic breast cancer cells MMTV-PyMT in the mammary fat pad. Mice that were treated pre-implantation with doxorubicin showed accelerated tumor growth and reduced survival rate, while mice treated with abemaciclib did not show significant differences when compared to control animals (Fig. 4j and Extended data Fig. 5f). Together, these data suggest that CDK4/6i treatment do not exert pro-tumorigenic and pro-frailty effects despite inducing senescence, possibly because CDK4/6i-induced senescence lacks a NASP.

Short-term abemaciclib treatment reduces the SASP of chemotherapy-induced senescence via p53

p53 is able to restrain the SASP[17], and drugs that promote p53 activity, such as nutlin-3a, have the capacity to induce irreversible arrest[14] without NASP (Extended data Fig.4c,d) but also to reduce NF-κB activity and the NASP level of cells induced to senescence by genotoxic stress[15]. Interestingly, in the plasma of breast cancer patients undergoing treatment with CDK4/6i, we observed that the level of NASP factors was slightly decreased compared to baseline (Fig. 3j). Thus, we decided to analyze the effect of treating senescent cells expressing NASP with CDK4/6i. Short-term abemaciclib treatment was sufficient to promote p53 (Fig. 5a) and reduce NF-κB (Fig. 5b) transcriptional activities, and downregulated the expression of several NASP factors in human fibroblasts induced to senescence by doxorubicin (Fig. 5c). NASP level of doxorubicin-treated cells was not reduced by abemaciclib treatment in human (Fig. 5d) and mouse (Fig. 5e) fibroblasts without functional p53, suggesting that down-regulation depended on p53 activity. As SASP inhibition driven by abemaciclib treatment was maintained for several days after drug removal (Fig. 5c), we then evaluated the effect of the treatment for doxorubicin- and SASP-mediated adverse reactions *in vivo*. p16-3MR mice were sequentially treated with doxorubicin and abemaciclib. Abemaciclib did not affect the bioluminescence of doxorubicin-treated mice, suggesting that senolysis (i.e. elimination of senescent cells) was not achieved (Fig. 5f,g). However, similar to cell culture, short-term treatment with abemaciclib was sufficient to reduce the level of NASP factors (Fig. 5h). A rescue of the doxorubicin-induced weight loss upon abemaciclib treatment was not observed (Fig. 5i), but physical performance of mice treated with abemaciclib was significantly improved, as shown by rotarod (Fig. 5j) and grip strength assay (Fig. 5k). Our data suggest that low-dose abemaciclib treatment is sufficient to reduce chemotherapy-induced NASP and some of its side effects, mainly via a p53-mediated restriction of NF-κB activity.

Discussion

Collectively, we show here that normal cells treated with CDK4/6 inhibitors enter a program of stable growth arrest which establishment is dependent on the transcriptional activity of tumor suppressor p53. Normal cells without functional p53 activate a partial senescent phenotype without permanent growth arrest, suggesting that intact p53 functions are necessary for a complete response to CDK4/6 inhibition. While non-cancerous cells are likely to have wild-type and functional p53, p53 mutations are observed in > 50% of human malignancies[31]. Interestingly, previous studies have reported that breast cancer patients carrying p53 mutations are more likely to respond poorly to CDK4/6i[20], and that breast cancer cells with wild-type p53 are more sensitive to radiotherapy[32]. Moreover, it was shown that malignant transformation of hematopoietic cells depend on CDK6-mediated repression of p53 activity, and that CDK6 inhibition could reverse this effect[33]. However, the genomic landscape of cancer cells remains highly heterogeneous and unstable, making the demonstration of a direct correlation between p53 activity and irreversible cell cycle arrest in tumors a challenging task. We also show that CDK4/6i-treated normal cells enter a senescent program characterized by morphological changes, suppression of many cell cycle-related genes, induction of a core senescence-associated signature and activation of lysosomal content and enzymes, but lacking many of the common SASP factors. Interestingly, we observe a clear distinction of two SASP programs: the NASP (NF-κB-associated secretory phenotype), which includes NF-κB targets, and the PASP (p53-associated secretory phenotype), which includes p53 targets. Treatment with CDK4/6i induces a PASP and not a NASP, which reflects the lack of chronic DDR and activation of NF-κB signaling, two essential regulators of the pro-inflammatory SASP[11,12]. In accordance to lacking several detrimental pro-inflammatory factors, prolonged abemaciclib treatment causes premature senescence *in vivo*, but the abemaciclib-induced senescent cells are extremely well tolerated. These data fit with the notion that toxicity of CDK4/6i in patients is generally lower than upon treatment with standard chemotherapy[34], despite the long-term treatment, and suggest that treatment with CDK4/6i could be better tolerated by cancer populations that are at high risk of developing side effects. Moreover, the presence *in vivo* of p16+ senescent cells with no SASP and detrimental effects emphasize how heterogeneous the senescence phenotype can be, and the importance of carefully phenotyping senescent cells to determine their potential toxicities. According to our data, one of the regulators of senescence-associated toxicities is predicted to be the NASP, while senescent cells with only PASP might be well-tolerated. Importantly, a previous study showed that abemaciclib could also potentiate tumor immunosurveillance[21], and our whole-transcriptome analysis suggest that abemaciclib-induced senescent cells upregulate several mediators of the interferon response. However, since senescent cells and the SASP have variable immune modulating effects[35–38], it remains to be assessed whether NASP and PASP are positively or negatively regulating immune responses. We also show that short-term

treatment with abemaciclib is sufficient to reduce chemotherapy-induced toxicity, suggesting the use of CDK4/6i for combinatorial interventions aimed at reducing chemotoxicity. The expression of doxorubicin-induced pro-inflammatory NASP factors was reduced in cells and mice upon abemaciclib treatment as a consequence of reduced NF-κB activity. A reduction of NF-κB is likely due to p53-mediated mechanisms, as we show here, and by the disruption of CDK6 activity, which was shown previously to regulate the expression of NF-κB-dependent genes[39]. Considering that CDK4/6i are already given to cancer patients that did not respond to chemotherapy, we believe that small adjustments in treatment regimen could have a profound pro-healthspan effect counteracting chemotherapy-induced adverse reactions.

Materials and Methods

Cell culture and drug administration

BJ (CRL-2522), WI38 (CRL-7728), MMTV-PyMT (CRL-3278), A549 (CCL-185), HCC827 (CRL-2868) and MCF7 (HTB-22) cells were purchased from ATCC. MEFs were generated from 13.5-day wild-type and $p16^{-/-}$ embryos. MDFs were isolated from the dorsal skin of 3-month-old p53-null mice or wild-type littermates and a gift from Prof. Paul Hasty (University of Texas Health Science Center at San Antonio, USA). Cells were not re-authenticated by the laboratory but were regularly monitored for mycoplasma contaminations (once per month). No cell line used was listed in the database of commonly misidentified cell lines maintained by ICLAC. All cells were cultured in DMEM-GlutaMAX (Thermo Fisher) medium supplemented with 10% fetal bovine serum (GE Healthcare Life Sciences) and 1% penicillin-streptomycin (Lonza). All the human and mouse normal primary cells were maintained in 5% O_2, 5% CO_2, 37 °C incubators and all cancer cells were maintained in 20% O_2, 5% CO_2, 37 °C incubators. For drug treatment experiments, cells were plated in 6-well dishes with 3 technical repeats ($3*10^4$ cells/well, around 30% confluence). Doxorubicin hydrochloride (Tebu-bio, BIA-D1202-1) was dissolved in sterile milliQ water at 250 μM as stock. Paclitaxel (MedChemExpress, HY-B0015) was dissolved in DMSO at 10 mM as stock. Palbociclib isethionate (Sigma-Aldrich, PZ0199) was dissolved in sterile milliQ water at 50 mM as stock. Abemaciclib (MedChemExpress, HY-16297) was dissolved in sterile milliQ water at 50 mM as stock. Nutlin-3a (MedChemExpress, HY-10029) was dissolved in DMSO at 10 mM as stock. Pifithrin-α hydrobromide (MedChemExpress, HY-15484) was dissolved in DMSO at 10 mM as stock All the drugs were further diluted in above-mentioned DMEM to treat cells at different concentrations as indicated in each figure legend.

Colony formation assay

Drug-treated normal or breast cancer cells were re-plated in a 6-well ($3*10^3$ cells/well) at the end of treatment, and allowed to grow in drug-free normal medium for 8 days; Cancer cells were plated in a 6-well ($3*10^4$ cells/well), and incubated with serum-free conditioned media (CM) for 45 hours. Afterwards, cells were fixed in 4% PFA for 30 minutes and then stained with 0.2% crystal violet in 37% methanol for 1 hour. Pictures of all the plates were taken with a scanner (Epson). The images were cropped and processed in Microsoft PowerPoint using the same settings.

EdU staining

Drug-treated cells were re-plated on coverslip in a 24-well plate ($3*10^4$ cells/well) and cultured for 10 or 20 hours in the presence of EdU (10 μM), then fixed and stained as previously described[40]. Images were acquired at 100

times magnification (Leica), and the number of cells was counted with the software ImageJ. The images were cropped using Microsoft PowerPoint.

Senescence-associated β-galactosidase staining

For staining of cells, drug-treated cells were re-plated in a 24-well plate ($2x10^4$ cells/well), and the SA-β-galactosidase staining was done as described previously (Hernandez-Segura et al., 2018a). For *in vivo* kidney section staining, kidneys from drug-treated and control animals were immediately imbedded in O.C.T (Sakura, 621232), snap-frozen in liquid nitrogen and stored in -80 ºC. The sectioning (10 µm) was done using cryostat one hour prior to staining, the slides washed with prechilled PBS on ice in a glass coplin jar twice for 5 minutes and fixed in a mixture of formaldehyde (2%) and gluteraldehyde (0.2%) for 10 minutes on ice. After fixation, the slides were washed briefly with milliQ water, and then stained with the staining buffer overnight in 37 ºC incubator without CO_2. The staining buffer included 1 mg/ml X-gal (Thermo Fisher) in dimethylformamide, 40 mM citric acid/Na phosphate buffer, 5 mM potassium ferrocyanide, 5 mM potassium ferricyanide, 150 mM sodium chloride and 2 mM magnesium chloride. Next day, the staining solution was washed away with milliQ water and the slides were mounted with 70% glycerol. Images were acquired at 100x magnification with a microscope (Leica) and were processed in Microsoft PowerPoint. The SA-β-gal positive area and total area was measured and quantified by with the software ImageJ.

Immunofluorescence

Cells were re-plated in 24-well dishes with coverslip ($3x10^4$ cells/well) and cultured in normal medium for 8 days. On the day of staining, the cells were gently washed with PBS for 3 times, fixed 10-15 minutes with 4% PFA, washed 3 times with PBS and permeabilized for 15 minutes with 0.1% Triton-100-X in PBS. After 3 washes with PBS, cells were blocked for 45 min in 3% BSA/PBS and incubated in primary antibody (gamma H2AX, 1:800 dilution; Novus, NB100-384) in 3% BSA/PBS at 4 ºC overnight. After 3 washes with PBS, coverslips were incubated with secondary antibody for 45 minutes in dark at room temperature and then with 2 µg/ml DAPI for 15 minutes in dark at room temperature. After washing 3 times, the samples were mounted with ProLong Gold Antifade Mountant (Thermo Fisher). Images were acquired at 100X magnification with a microscope (Leica).

Conditioned media (CM) collection and analyses

BJ fibroblasts were treated with vehicle (water - 8 times 24 hours; 1 in 1,000), doxorubicin (250 nM – 1 time 24 hours) or abemaciclib (1 µM - 8 times 24 hours). After the treatments, cells were cultured with drug-free normal medium for 8 days. Thereafter, cells from different groups were trypsinized and counted, and 10^6 cells from each group were re-plated and incubated with serum-free medium for 24 hours. Then the CM was collected and

centrifuged at 300 g / 5 minutes to remove any floating cell or debris. The CM was kept in -80 ºC after harvesting and thawed on ice for further analyses or experiments. Human Cytokine Antibody Array (Abcam, ab133997) was used following manufacturer's instructions. After the images were taken, density of positive controls from 4 membranes was equalized using Adobe Photoshop, and individual factors from different membranes compared. For ELISA, human CXCL1/GROα duo-set or CCL5 duo-set or IGFBP3 duo-set (R&D Systems) were used to detect the concentrations of CXCL1 or CCL5 or IGFBP3 in the CM following manufacturer's instructions.

Western blot

Total cell lysates were obtained by resuspension of the cells in RIPA buffer (cat# ab156034, Abcam) supplemented with proteinase and phosphatase inhibitors (cat# A32959, Pierce (TFS)). Protein concentration was measured using a BCA protein assay kit (cat# 10741395, Pierce (TFS)) and subsequently protein sample buffer was added to a final concentration of 40 mM Tris-HCl (pH 6.8), 1.9% SDS, 3.1% β-mercaptoethanol and 6,3% glycerol. Samples were boiled for 5 minutes. Equal amount of proteins was loaded onto 12% SDS-PAGE gel (acrylamide : bis-acrylamide 29:1, cat# 161-0146, Bio-Rad) and after size separation blotted onto 0.2 µm nitrocellulose membrane (cat# 162-0112, Bio-Rad). Immunodetection was performed by standard procedures of p16/Ink4a (clone EPR1473, cat# ab108349, Abcam), p21 (clone C-19, cat# sc-397, Santa Cruz Biotechnology), p53 (clone DO-1, cat# sc-126, Santa Cruz Biotechnology), Ser15-p53 (Cat# 9284S, Cell Signaling Technology), Rb (clone 4H1, cat# 9309, Cell Signaling Technology), phospho-Rb (ser795, cat# 9301, Cell Signaling Technology) and HMGB1 (cat# ab18256, Abcam). The antibodies for the proteins of interest were used in 1:1000 dilution in 5%milk/TBST (Tris-buffered Saline with 0.1% Tween20) and incubated overnight at 4 degrees Celsius. Immunodetection of vinculin (cat# V9131, Sigma-Aldrich) or β-Actin (clone C4, cat# 08691001, MP Biomedicals) was performed as loading control. ECL Prime western blotting detection reagent (cat# RPN2232, GE Healthcare) was used according to manufacturer's guidelines for detection and the signal was measured using an ImageQuant LAS 4000 biomolecular imager (GE Healthcare). Densitometry was performed using ImageJ software (NIH – Public domain) and values were corrected for protein input as measured by the loading control.

Generation of a lentiviral NF-κB reporter vector

Plasmid pGL4.32[luc2P/NF-κB-RE/Hygro] (cat# E8491, Promega) was used as template DNA in a PCR for obtaining the minimal promoter Luc2P together with the NF-κB response elements (NF-κB-RE). The DNA polymerase used was Phusion High Fidelity (cat# E0553S, New England Biolabs (NEB)). Forward primer: 5'-aaaaATCGATgg cctaactggccggtacc-3', reverse primer 5'-aaaaGGATCCcgactctagagtcgcggcc-3'. The PCR product was purified from gel cut with ClaI (cat#10656291001, Roche) and BamHI-HF (cat# R3136s, NEB)

overnight at 16 degrees Celsius. This fragment was ligated into the backbone vector pLenti CMV GFP Hygro (656-4) (restriction with ClaI and BamHI-HF released the CMV promoter from the lentiviral backbone sequence). pLenti[CMV/GFP/Hygro] (656-4) was a gift from Eric Campeau & Paul Kaufman (Addgene plasmid #17446). The cut backbone vector was treated with Antarctic Phosphatase (cat# M0289S, NEB) before ligation. T4 DNA ligase (cat# M0202S, NEB) was used in the ligation reaction. All enzymes were used according to manufacturer's manual. The ligation reaction products were transformed into NEB stable Competent *E. coli* (High Efficiency, cat# c3040h, NEB) and grown overnight at 37 degrees Celsius on LB plates supplemented with 50 µg/ml Ampicillin. A colony PCR was performed to check for positive clones. Single positive clones were grown overnight in liquid LB supplemented with Ampicillin at 37 degrees Celsius to be midiprepped the next day using a PureLink® HiPure Plasmid Midiprep Kit (cat# K210005, Invitrogen). This newly generated lentiviral NF-κB-reporter vector (pLenti-NF-κB-RE-minP-LUC-EGFP-hygro) was send to GATC/Eurofins for sequencing and verification of the Luc2P/ NF-κB-RE insert. Recombinant human TNF-α (PeproTech, 300-01A) (10 ng/µl; 6 hours treatment) was used as positive control to validate the NF-κB reporter.

Generation of a lentiviral p53-reporter vector

Plasmid PG13-luc (wt p53 binding sites) was used as template DNA in a PCR for obtaining the p53 wild-type binding sites together with the luciferase reporter. PG13-luc (wt p53 binding sites) was a gift from Bert Vogelstein (Addgene plasmid # 16442). The DNA polymerase used was Phusion High Fidelity (cat# E0553S, NEB). Forward primer 5'-aaaaaGGGACCCaaaCGATAAGCTTGATGCC-3', reverse primer 5'-tttttGTCGACaaaTTAAATCTC TGTAGG-3'. The PCR product was purified from gel and cut with KflI (cat# FD2164, ThermoFisher Scientific) and SalI (cat# R3138, NEB) for 15 minutes at 37 degrees Celsius. This cut PCR product was ligated into the backbone vector pLenti CMV GFP Hygro (656-4) (restriction with KflI ans SalI releases the cPPT/CST element, the CMV promoter and the EGFP from the lentiviral backbone sequence. The cut backbone vector was treated with Antarctic Phosphatase (cat# M0289S, NEB) before ligation. T4 DNA ligase (cat# M0202S, NEB) was used in the ligation reaction. All enzymes were used according to manufacturer's manual. The ligation reaction products were transformed into NEB stable Competent *E. coli* (High Efficiency, cat# c3040h, NEB) and grown overnight at 37 degrees Celsius on LB plates supplemented with 50 µg/ml Ampicillin. A colony PCR was performed to check for positive clones. Single positive clones were grown overnight in liquid LB supplemented with Ampicillin at 37 degrees Celsius to be midiprepped the next day using a PureLink® HiPure Plasmid Midiprep Kit (cat# K210005, Invitrogen). This newly generated intermediate lentiviral p53-reporter vector (pLenti–p53 WT bind. sites-LUC-hygro) was still dysfunctional because of lacking the cPPT/CST element. The cPPT/CST element has

been repaired before the newly generated lentiviral p53-reporter vector (pLenti–p53 WT bind.sites-LUC-hygro) was sent to GATC/Eurofins for sequencing and verification of the cPPT/CST-p53 WT bind.sites-LUC insert. Nutlin-3a (MedChemExpress, HY-10029) (10 µM; 24 hours treatment) was used as positive control to validate the p53-reporter.

Production of lentivirus

293FT cells were seeded in a 10 cm petridish at $6*10^6$ cells. Next day, cells were transfected with the ViraPower plasmid mix (cat# K4970-00, Invitrogen) together with the lentiviral vectors using PolyFect transfection reagent (cat# 301105, Qiagen) overnight. The medium with transfection mix was replaced for normal growth medium without antibiotics, collected after 24 hours and concentrated using Peg-It Virus precipitation solution (cat# LV810A-1, System Biosciences) according to the manufacturer's manual.

Lentivirus transduction

Lentiviral particles were either generated by the laboratory (NF-κB or p53 reporter) or obtained from the MISSION shRNA library (Sigma-Aldrich). These obtained lentiviral particles harbor the following shRNA clones in pLKO.1 backbone vector and were used to infect BJ cells: p16 (*CDKN2A-INK4A*)–TRCN0000255853; p53 (*TP53*)–TRCN0000003755. Titers of these lentiviral particles were all equal to or higher than 1.8E+07 TU/ml. 10^5 BJ cells per well were seeded in a 6 well plate format on day 0. On day 1, cells were infected with the lentiviral particles (1:20 dilution in complete medium) for 24 hrs. Polybrene (6 µg/ml; cat# sc-134220, Santa Cruz Biotechnology) was added together with the lentiviral particles to enhance the infection efficiency. Cells were washed and refreshed with complete medium on day 2. Selection with puromycin (2 µg/ml; cat# P8833, Sigma-Aldrich) started on day 3 for 3 days. BJ cells infected with pLKO.1-scrambled lentiviral particles were used to serve as control cells.

RNA sequencing assay

Total RNA was extracted from treated cells via an ISOLATE II RNA mini kit (Bioline, Cat: BIO-52073) following manufacturer's instructions. The extracted RNA was quantitated using a Nanodrop and RNA quality was measured via BioAnalyzer RNA chip (Agilent). Poly-A tail selection was used to enrich for messenger RNA (mRNA) using the NEXTflex Poly(A) Beads kit (Bioo Scientific Corp, cat #512980). RNA-Seq library preparation was carried out using NEXTflex Rapid Directional qRNA-Seq kit (Bioo Scientific, cat# 5130-05D). In brief, mRNA was fragmented using a cationic buffer and then submitted to first and second strand synthesis, followed by adenylation, ligation and 15 cycles of PCR. Library quality and size distribution were validated on a Qubit (Thermo Fisher Scientific) and an Agilent High Sensitivity DNA chip. Clusters for sequencing were generated on the cBot

(Illumina). Paired-end sequencing was performed at 400 M reads per lane of the flow cell on an Illumina HiSeq 2500. Average quality scores for the completed run across all samples was >30, with an average of 10 million reads for each pooled sample. The read length was 76 bp. Raw sequencing data were demultiplexed according to library-specific barcodes and converted to fastq format using standard Illumina software (bcl2fastq version 1.8.4). The resulting reads were mapped to the human reference genome (GRCh38) using Bowtie2 (version 2.2.4). Sequencing data is available on ArrayExpress under accession no. **E-MTAB-7642**. For differential gene expression, we used DESeq2[41] to evaluate the genes that were differentially expressed among all the different treatments compared to the vehicle-treated control. We considered those genes with an adjusted p-value lower than 0.01 as being differentially expressed. A profile of senescence associated secretory phenotype (SASP) genes was generated based on literature and previous knowledge, detailed information provided as in **supplementary table S2**. GraphPad Prism 7 was used to generate the heat-map using the logarithm base 2 of fold change. Enriched pathways in the differentially expressed genes were evaluated using the online tool "Over-representation analysis" of the Consensus Path DB-human (http://cpdb.molgen.mpg.de/)[42]. For the Venn plots showing similarly expressed genes in different conditions, only genes that were differentially expressed with a fold change in the same direction (up- or down-regulated in samples compared) were considered. Venn plots were generated in R version 3.5.1 using the packages "VennDiagram".

qRT-PCR assay

Total RNA was isolated using an Isolate II Rna Mini Kit (Bioline). 250~500 ng of RNA was reverse transcribed into cDNA using the High-Capacity cDNA reverse transcription kit (Applied Biosystems). qRT-PCR reactions were performed using the Universal Probe Library system (Roche) and a SensiFast Probe kit (Bioline). Expression of tubulin was used to normalize the expression of target genes. Every biological replicate was analyzed in duplicate. List of primers is provided in **supplementary table S3**.

Chromatin immunoprecipitation (ChIP) assay

BJ cells treated with vehicle, abemaciclib (1 µM - 8 times 24 hours) or nutlin-3a (10 µM - 8 times 24 hours) were crosslinked and processed using the ChIP kit (ab500, Abcam) following manufacturer's instructions. 6 rounds of sonication (high energy, 30 seconds on / 30 seconds off) was done using a sonicator. After DNA was purified, qRT-PCR was done with SYBR green super mix (1725120, Biorad) using primers as followed:

CDKN1A #1	Forward	*GGAGGCAAAAGTCCTGTGTTC*	(Saramäki et al., 2006)
	Reverse	*GGAAGGAGGGAATTGGAGAG*	
CDKN1A #2	Forward	*GAAATGCCTGAAAGCAGAGG*	
	Reverse	*GCTCAGAGTCTGGAAATCTC*	

CDKN1A #3	Forward	*CACCACTGAGCCTTCCTCAC*	
	Reverse	*CTGACTCCCAGCACACACTC*	
CDKN1A #4	Forward	*GATGCCAACCAGATTTGCCG*	
	Reverse	*CCTGGCTCTAACAACATCCC*	
MDM2	Forward	*GGTTGACTCAGCTTTTCCTCTTG*	(Jackson and Pereira-Smith, 2006)
	Reverse	*GGAAAATGCATGGTTTAAATAGCC*	
GADD45A	Forward	*AGCGGAAGAGATCCCTGTGA*	
	Reverse	*CGGGAGGCAGGCAGATG*	
IGFBP3	Forward	*CGAGCCCCTGAGGCAAA*	
	Reverse	*GCTTGGTGTCCAGCTCAGATG*	

Transwell migration assay

MCF7 breast cancer cells ($2*10^4$) were re-suspended in serum–free medium and seeded in a transwell insert (8 µm pore, Corning) with serum-free media collected from drug-induced senescent fibroblasts in the outer chamber of a 24-well culture dish. Cells were cultured in a 5% O_2, 5% CO_2, 37 ºC incubator for 16 hours. Thereafter, cells migrated to the lower side of the trans-well were fixed with 4% PFA and stained with 0.2% crystal violet. Images were acquired at 40X magnification with a microscope (Leica).

Scratch migration assay and IncuCyte imaging

A549 lung cancer cells ($4*10^4$) were plated in a 96-well ImageLock plate (Sartorius) and cultured in a 20% O2, 5% CO2, 37 ºC incubator for 24 hours. Then the 96-pin IncuCyte WoundMaker was used to create precise and reproducible cell-free zone in each well. Cells were washed with PBS and then incubated with serum-free conditioned media collected from drug-induced senescent fibroblasts for 24 hours in the IncuCyte imaging machine. Images were taken every 2 hours and analyzed by the IncuCyte software.

***In vivo* animal experiments**

All the mice were maintained in the central animal facility (CDP) of University Medical Center Groningen (UMCG) under standard conditions. All the experiments were approved by the Central Authority for Scientific Procedures on Animals (CCD – License #AVD105002015339 and #AVD1050020184807) in the Netherlands.

For abemaciclib anti-tumor effect validation, 10^6 fLUC-MMTV-PyMT cancer cells, previously generated (Demaria et al., 2017), were injected into the mammary fat pad of 13-week-old female p16-3MR mice under anesthesia (10 mice). At 7 days and 14 days post cell injection, the mice were injected with 150 mg/kg D-Luciferin (Sanbio, 14681-1). 8 minutes later, the mice were anesthetized with 2% isoflurane and firefly bioluminescence was visualized/quantified using the IVIS Spectrum *In Vivo* Imaging System (PerkinElmer, 5-minute medium binning) in CDP-UMCG. The mice were equally distributed in two groups based on tumor size (bioluminescence).

The female mice bearing breast cancer were then injected i.p. with vehicle (PBS, 7 consecutive days) or abemaciclib (in PBS, 50 mg/kg, 7 consecutive days) (n=5 mice/group). After the second bioluminescence imaging, the mice were terminated, and tumors were excised for weighing.

For senescence induction and healthspan analysis in p16-3MR, both male and female mice were used. 14-week-old healthy mice were injected i.p. with vehicle (PBS, 7 consecutive days), doxorubicin (in PBS, 5 mg/kg, 3 consecutive days) or abemaciclib (in PBS, 50 mg/kg, 7 consecutive days) (n=6 mice/group). All the treatments were finished at the same day. At 14 days post above-mentioned treatments, the mice were injected with 100 µl Xenolight RediJect Coelenterazine h (PerkinElmer, 760506). 20 minutes post injection, mice were anesthetized with 2% isoflurane and renilla bioluminescence was visualized/quantified by the IVIS Spectrum *In Vivo* Imaging System (PerkinElmer, 5-minute medium binning) in CDP-UMCG. Forelimb grip strength (N) was measured using a grip strength meter (Columbus Instruments) at 7 and 14 days post treatments, and results were averaged from 5 trials. Hanging tests were performed at 7 and 14 days post treatments. The mice were placed under the grid of above-mentioned grip strength meter with the bedding below to protect the mice when they fell down. A cut-off time of 300 seconds was determined, and the hanging time was normalized to body weights as hanging duration (sec) multiplied by body weight (g). At 15 days post treatments, endurance tests were performed on an accelerating RotaRod (IITC Life Science) using a top speed of 40 r.p.m. over a period of 300 seconds. Each mouse was put on the machine to adapt twice, four hours later two trials were recorded for each mouse. The average of the two trials was calculated and plotted. For *ex vivo* analysis, kidneys and livers were both snap-frozen in liquid nitrogen for RNA/protein isolation and imbedded in O.C.T (Sakura, 621232) (frozen in liquid nitrogen) for cryo-sectioning. All the samples were stored in -80 ºC until analyzed. 20 µg total protein was collected from each treated kidney and IL6 protein level was determined by the mouse IL6 duo-set (R&D Systems) ELISA. The experiments were done following manufacturer's instructions. Part of the plasma was used for *in vivo* ELISA, 100 µl plasma from each mouse was tested using the mouse CXCL1/KC duo-set (R&D Systems). The experiments were done following manufacturer's instructions. Around 25 µl of plasma was diluted and used for red blood cell and white blood cell counting (Medonic CA620). Around 900 µl of plasma from each mouse was used to stain for T cell (1:150, APC-CD3e/clone 145-2C11, Biolegend Cat.100312), B cell (1:300, FITC-CD45R/B220/clone RA3-6B2, Biolegend Cat.103205), granulocyte and macrophage (1:1000, PECy7-Gr-1/clone RB6-8C5 and PECy7-CD11b /clone M1/70, Biolegend Cat.108416 and Cat.101216), then analyzed by flow cytometry (BD MoFlo XDP).

For abemaciclib+ pifithrin-α experiments in p16-3MR, both male and female mice were used. 14-week-old healthy mice were injected i.p. with abemaciclib (in PBS, 50 mg/kg, 7 consecutive days) + vehicle (5% DMSO in PBS)

or abemaciclib + pifithrin-α (5% DMSO in PBS, 2 mg/kg, 7 consecutive days) (n=5 mice/group). All the treatments were finished at the same day. At 20 days post above-mentioned treatments, the mice were injected with 100 µl Xenolight RediJect Coelenterazine h (PerkinElmer, 760506). 20 minutes post injection, mice were anesthetized with 2% isoflurane and renilla bioluminescence was visualized/quantified by the IVIS-100 *In Vivo* Imaging System (PerkinElmer, 5-minute medium binning) in CDP-UMCG. For *ex vivo* analysis, tissues were snap-frozen in liquid nitrogen for RNA/protein isolation. All the samples were stored in -80 °C until analyzed.

For MMTV-PyMT cancer cell injection in doxorubicin/abemaciclib-treated mice, 14-week-old healthy female mice were injected i.p. with vehicle (PBS, 7 consecutive days; n=6 mice), doxorubicin (in PBS, 5 mg/kg, 3 consecutive days; n=7 mice) or abemaciclib (in PBS, 50 mg/kg, 7 consecutive days; n=6 mice). All the treatments were finished at the same day. At 7 days post above-mentioned treatments, $3*10^5$ fLUC-MMTV-PyMT cancer cells were injected into the mammary fat pad of the treated female mice under anesthesia. The tumors were allowed to grow for 21 days. Then the mice were terminated, and tumors were excised for weighing and photos.

For human senescent/cancer cells co-injection in *Foxn1*^{Nu} mice, BJ fibroblasts were treated with vehicle (water for 8 times 24 hours; 1 in 1,000), doxorubicin (250 nM for 24 hours), palbociclib or abemaciclib (both 1 µM for 8 times 24 hours) *in vitro*. At 8 days post drug removal, BJ cells ($2.5*10^5$) from each group were co-injected with A549 cancer cells (10^6) subcutaneously in right flanks of 12-week-old female *Foxn1*^{Nu} mice (The Jackson Laboratory). 7 days after cell injection, tumor volume was calculated twice a week. The tumor length, width and depth were measured with a caliper and the investigator was blinded. The mice were terminated when one of the tumors reached the size for humane endpoint (>1,500 mm^3). After the tumors were excised, the weight of each tumor was measured and plotted.

For doxorubicin + abemaciclib sequential treatment analysis, female mice were used. 14-week-old healthy mice were injected i.p. with vehicle (3 consecutive days with PBS + 6 days of holiday + 3 consecutive days with PBS; n=6 mice), doxo+vehicle (in PBS; 3 consecutive days with 5 mg/kg doxorubicin + 6 days of holiday + 3 consecutive days with PBS; n=7 mice) or doxo+abema (in PBS; 3 consecutive days with 5 mg/kg doxorubicin + 6 days of holiday + 3 consecutive days with 50 mg/kg abemaciclib; n=7 mice). All the treatments were finished at the same day. At 14 days post doxorubicin treatments, Forelimb grip strength (N) was measured using a grip strength meter (Columbus Instruments), and results were averaged from 5 trials. At 15 days post treatments, endurance tests were performed on an accelerating RotaRod (IITC Life Science) using a top speed of 40 r.p.m. over a period of 300 seconds. Each mouse was put on the machine to adapt twice, four hours later three trials were recorded for each mouse. The average of the three trials was calculated and plotted. At 16 days post doxorubicin

treatments, the mice were injected with 100 µl Xenolight RediJect Coelenterazine h (PerkinElmer, 760506). 20 minutes post injection, mice were anesthetized with 2% isoflurane and renilla bioluminescence was visualized/quantified by the IVIS Spectrum *In Vivo* Imaging System (PerkinElmer, 5-minute medium binning) in CDP-UMCG. For *ex vivo* analysis, tissues were snap-frozen in liquid nitrogen for RNA/protein isolation. All the samples were stored in -80 ºC until analyzed.

Patient characteristics and plasma analysis

Paired plasma samples before start of therapy (pre-treatment) and after ±4 weeks (median 29 days) of treatment (on-treatment) were obtained from 9 metastatic breast cancer patients who received palbociclib treatment and 10 metastatic breast cancer patients who received paclitaxel treatment. Written informed consent was obtained from all patients. Mean age was 55.9 years (SD 10.9) for the palbociclib group and 60.1 years (SD 7.4) for the paclitaxel group. The samples were collected in cell stabilizing blood collection tubes (CellSave or Streck Cell-Free DNA BCT tubes). After collection the blood was centrifuged twice (1700 g for 10 minutes and 12000 g for 10 minutes). Afterwards the plasma was pooled and directly stored in 2 ml tubes in -80 ºC until analyzed. For ELISA, human CXCL1/GROα duo-set or CCL5 duo-set or IGFBP3 duo-set (R&D Systems) were used to detect the concentrations of CXCL1 or CCL5 or IGFBP3 in the plasma following manufacturer's instructions.

Statistics

Graphpad Prism 7 was used for the statistical analyses. Detailed information is provided in each figure legend.

References:

1. Hanahan, D. & Weinberg, R. Hallmarks of Cancer: The Next Generation. *Cell* **144**, 646–674 (2011).

2. Schmitt, C. Senescence, apoptosis and therapy — cutting the lifelines of cancer. *Nat Rev Cancer* **3**, 286–295 (2003).

3. Hernandez-Segura, A., Nehme, J. & Demaria, M. Hallmarks of Cellular Senescence. *Trends Cell Biol* **28**, 436–453 (2018).

4. Rodier, F. & Campisi, J. Four faces of cellular senescence. *J Cell Biology* **192**, 547–556 (2011).

5. Sun, Y. *et al*. Treatment-induced damage to the tumor microenvironment promotes prostate cancer therapy resistance through WNT16B. *Nat Med* **18**, 1359–1368 (2012).

6. Demaria, M. *et al*. Cellular Senescence Promotes Adverse Effects of Chemotherapy and Cancer Relapse. *Cancer Discov* **7**, 165–176 (2017).

7. Murali, B. *et al*. Inhibition of the Stromal p38MAPK/MK2 Pathway Limits Breast Cancer Metastases and Chemotherapy-Induced Bone Loss. *Cancer Res* **78**, 5618–5630 (2018).

8. Yao, Z. *et al*. Therapy-Induced Senescence Drives Bone Loss. *Cancer Res* **80**, 1171–1182 (2020).

9. Ferrucci, L. & Fabbri, E. Inflammageing: chronic inflammation in ageing, cardiovascular disease, and frailty. *Nat Rev Cardiol* **15**, 505–522 (2018).

10. Pierce, B. *et al*. Elevated Biomarkers of Inflammation Are Associated With Reduced Survival Among Breast Cancer Patients. *J Clin Oncol* **27**, 3437–3444 (2009).

11. Chien, Y. *et al*. Control of the senescence-associated secretory phenotype by NF-κB promotes senescence and enhances chemosensitivity. *Gene Dev* **25**, 2125–2136 (2011).

12. Rodier, F. *et al*. Persistent DNA damage signalling triggers senescence-associated inflammatory cytokine secretion. *Nat Cell Biol* **11**, 973–979 (2009).

13. Coppé, J. *et al*. Tumor Suppressor and Aging Biomarker p16INK4a Induces Cellular Senescence without the Associated Inflammatory Secretory Phenotype. *J Biol Chem* **286**, 36396–36403 (2011).

14. Efeyan, A. *et al*. Induction of p53-Dependent Senescence by the MDM2 Antagonist Nutlin-3a in Mouse Cells of Fibroblast Origin. *Cancer Res* **67**, 7350–7357 (2007).

15. Wiley, C. *et al*. Small-molecule MDM2 antagonists attenuate the senescence-associated secretory phenotype. *Sci Rep-uk* **8**, 2410 (2018).

16. Christy, B. *et al*. p53 and rapamycin are additive. *Oncotarget* **6**, 15802–15813 (2015).

17. Coppé, J. *et al*. Senescence-Associated Secretory Phenotypes Reveal Cell-Nonautonomous Functions of Oncogenic RAS and the p53 Tumor Suppressor. *Plos Biol* **6**, e301 (2008).

18. Finn, R. *et al*. Palbociclib and Letrozole in Advanced Breast Cancer. *New Engl J Medicine* **375**, 1925–1936 (2016).

19. Goetz, M. *et al*. MONARCH 3: Abemaciclib As Initial Therapy for Advanced Breast Cancer. *J Clin Oncol* **35**, JCO.2017.75.615 (2017).

20. Patnaik, A. *et al.* Efficacy and Safety of Abemaciclib, an Inhibitor of CDK4 and CDK6, for Patients with Breast Cancer, Non–Small Cell Lung Cancer, and Other Solid Tumors. *Cancer Discov* **6**, 740–753 (2016).

21. Goel, S. *et al.* CDK4/6 inhibition triggers anti-tumour immunity. *Nature* **548**, 471–475 (2017).

22. Yoshida, A., Lee, E. & Diehl, J. Induction of Therapeutic Senescence in Vemurafenib-Resistant Melanoma by Extended Inhibition of CDK4/6. *Cancer Res* **76**, 2990–3002 (2016).

23. Yang, C. *et al.* Acquired CDK6 amplification promotes breast cancer resistance to CDK4/6 inhibitors and loss of ER signaling and dependence. *Oncogene* **36**, 2255–2264 (2017).

24. Hernandez-Segura, A. *et al.* Unmasking Transcriptional Heterogeneity in Senescent Cells. *Curr Biol* **27**, 2652-2660.e4 (2017).

25. Demaria, M. *et al.* An Essential Role for Senescent Cells in Optimal Wound Healing through Secretion of PDGF-AA. *Dev Cell* **31**, 722–733 (2014).

26. Fischer, M. Census and evaluation of p53 target genes. *Oncogene* **36**, 3943–3956 (2017).

27. Spurgers, K. *et al.* Identification of Cell Cycle Regulatory Genes as Principal Targets of p53-mediated Transcriptional Repression. *J Biol Chem* **281**, 25134–25142 (2006).

28. Mittelman, J. & Gudkov, A. Generation of p53 Suppressor Peptide From the Fragment of p53 Protein. *Somat Cell Molec Gen* **25**, 115–128 (1999).

29. Sohn, D. *et al.* Pifithrin-α protects against DNA damage-induced apoptosis downstream of mitochondria independent of p53. *Cell Death Differ* **16**, 869–878 (2009).

30. Andersson, U. & Tracey, K. HMGB1 Is a Therapeutic Target for Sterile Inflammation and Infection. *Annu Rev Immunol* **29**, 139–162 (2011).

31. Muller, P. & Vousden, K. p53 mutations in cancer. *Nat Cell Biol* **15**, 2–8 (2013).

32. Fernández-Aroca, D. *et al.* P53 pathway is a major determinant in the radiosensitizing effect of Palbociclib: implication in cancer therapy. *Cancer Lett* **451**, 23–33 (2019).

33. Bellutti, F. *et al.* CDK6 antagonizes p53-induced responses during tumorigenesis. *Cancer Discov* **8**, CD-17-0912 (2018).

34. Klein, M., Kovatcheva, M., Davis, L., Tap, W. & Koff, A. CDK4/6 Inhibitors: The Mechanism of Action May Not Be as Simple as Once Thought. *Cancer Cell* **34**, 9–20 (2018).

35. Iannello, A. & Raulet, D. Immune Surveillance of Unhealthy Cells by Natural Killer Cells. *Cold Spring Harb Sym* **78**, 249–257 (2013).

36. Stokes, K. *et al.* Natural killer cells limit the clearance of senescent lung adenocarcinoma cells. *Oncogenesis* **8**, 24 (2019).

37. Ventura, A. *et al.* Restoration of p53 function leads to tumour regression in vivo. *Nature* **445**, 661–665 (2007).

38. Xue, W. *et al.* Senescence and tumour clearance is triggered by p53 restoration in murine liver carcinomas. *Nature* **445**, 656–660 (2007).

39. Handschick, K. *et al.* Cyclin-Dependent Kinase 6 Is a Chromatin-Bound Cofactor for NF-κB-Dependent Gene Expression. *Mol Cell* **53**, 193–208 (2014).

40. Hernandez-Segura, A., Brandenburg, S. & Demaria, M. Induction and Validation of Cellular Senescence in Primary Human Cells. *J Vis Exp Jove* (2018) doi:10.3791/57782.

41. Love, M., Huber, W. & Anders, S. Moderated estimation of fold change and dispersion for RNA-seq data with DESeq2. *Genome Biol* **15**, 550 (2014).

42. Kamburov, A., Stelzl, U., Lehrach, H. & Herwig, R. The ConsensusPathDB interaction database: 2013 update. *Nucleic Acids Res* **41**, D793–D800 (2013).

Acknowledgments:

We thank Bertien Dethmers and Gerald de Haan for help with blood analysis and Britt Sterken and Cornelis F Calkhoven for help with breast cancer cell experiments. We are thankful to the Demaria laboratory for fruitful discussions.

Funding:

This work was supported by the University Medical Center Groningen and by a grant from the Dutch Cancer Foundation (KWF) to M.D.

Author Contributions:

Conceptualization: B.W. and M.D.; **Data curation**: B.W. and M.D.; **Formal analysis**: B.W., A.H.-S. and M.D.; **Funding acquisition**: M.D.; **Investigation**: B.W., S.B., A.H.-S., T.V. and L.J.; **Methodology**: B.W., A.H.-S. and M.D.; **Project administration**: B.W. and M.D.; **Resources**: B.W., A.H.-S., N.O., S.W., A.J. and M.D.; **Supervision**: M.D.; **Validation**: B.W., S.B., A.H.-S., T.V. and M.D.; **Visualization**: B.W. and M.D.; **Writing – original draft**: B.W. and M.D.; **Writing – review & editing**: B.W., S.W., A.J., N.O. and M.D..

Declaration of Interests:

M.D. is scientific co-founder, advisor and shareholder of Cleara Biotech.

Figures and legends

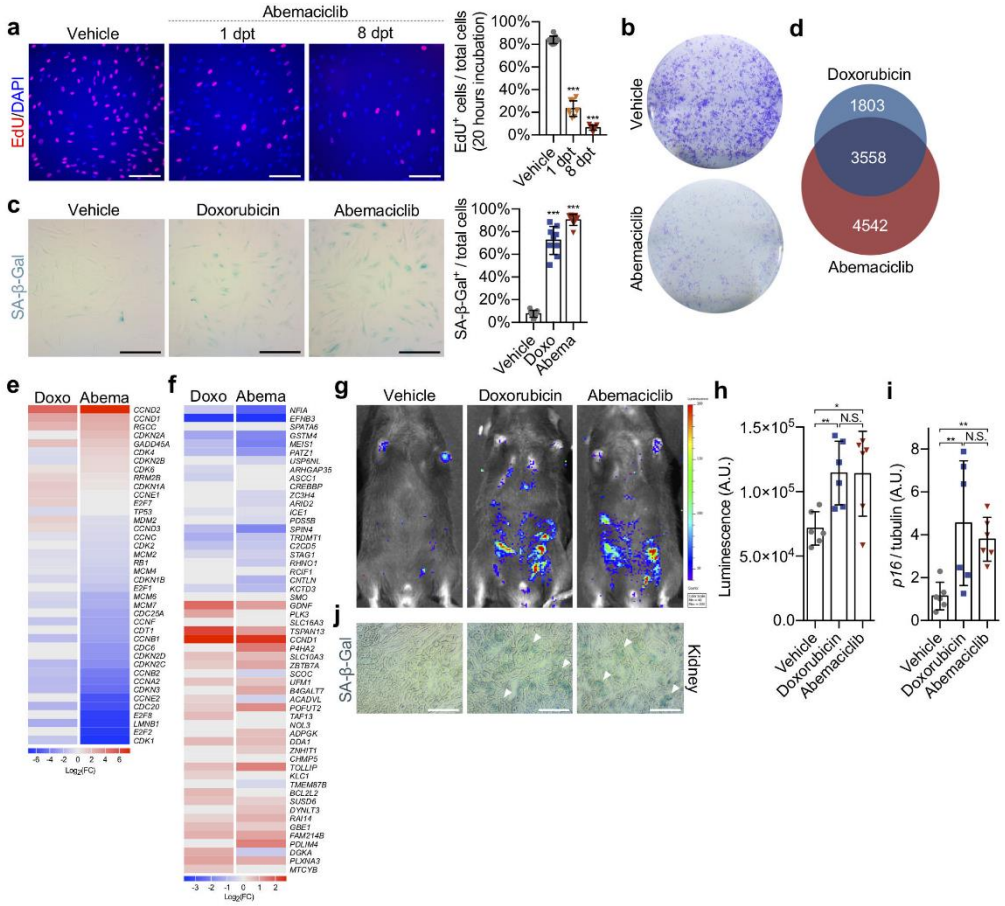

Figure 1. Long-term CDK4/6i treatment induces cellular senescence in human cells and cancer-free mice. **a-f**, Human fibroblasts (BJ) were treated with vehicle (water for 8 times 24 hours), abemaciclib (1 µM for 1 or 8 times 24 hours) or doxorubicin (250 nM for 24 hours). 1 or 8 dpt, cells were incubated with EdU for 20 hours and stained and quantified (n=9 samples from 3 independent experiments; scale bar, 150 µm) (**a**). $3x10^3$ cells treated with vehicle or abemaciclib were re-plated for colony formation assay after drug withdraw and stained with 0.2% crystal violet (n=3 independent experiments) (**b**). 8 dpt, cells were stained for SA-β-gal and quantified (n=9 samples from 3 independent experiments; scale bar, 1 mm) (**c**). Venn plot of RNA-sequencing datasets of treated cells at 8 dpt (n=3 independent samples, sequenced together) (**d**). Heatmap of cell cycle genes (**e**) or the senescence-associated signature (**f**) for doxorubicin- or abemaciclib-treated groups (8 dpt) relative to vehicle-treated group from the RNA-sequencing datasets (p-value<0.01 was regarded as significant). **g-j**, p16-3MR mice were treated with vehicle (PBS, 7 consecutive days), doxorubicin (5 mg/kg, 3 consecutive days) or abemaciclib (50 mg/kg, 7 consecutive days). n=6 mice/group. 14 dpt, bioluminescence was visualized and quantified by the IVIS spectrum *in vivo* imaging system, as shown by representative bioluminescence images (**g**) and quantification (**h**). RNA isolated from kidneys and mRNA encoding p16 quantified by qRT-PCR (**i**). Representative images to visualize SA-β-gal activities in vehicle-, doxorubicin- or abemaciclib-treated mouse kidney sections at 15 dpt (arrows indicated positive area; scale bar, 1 mm; n=3) (**j**). One-way ANOVA, data are means ± s.d. (**a**,**c**, **h** and **i**). *p<0.05, **p<0.01, ***p<0.001, N.S.=not significant. dpt, days post treatment. Doxo, doxorubicin. Abema, abemaciclib.

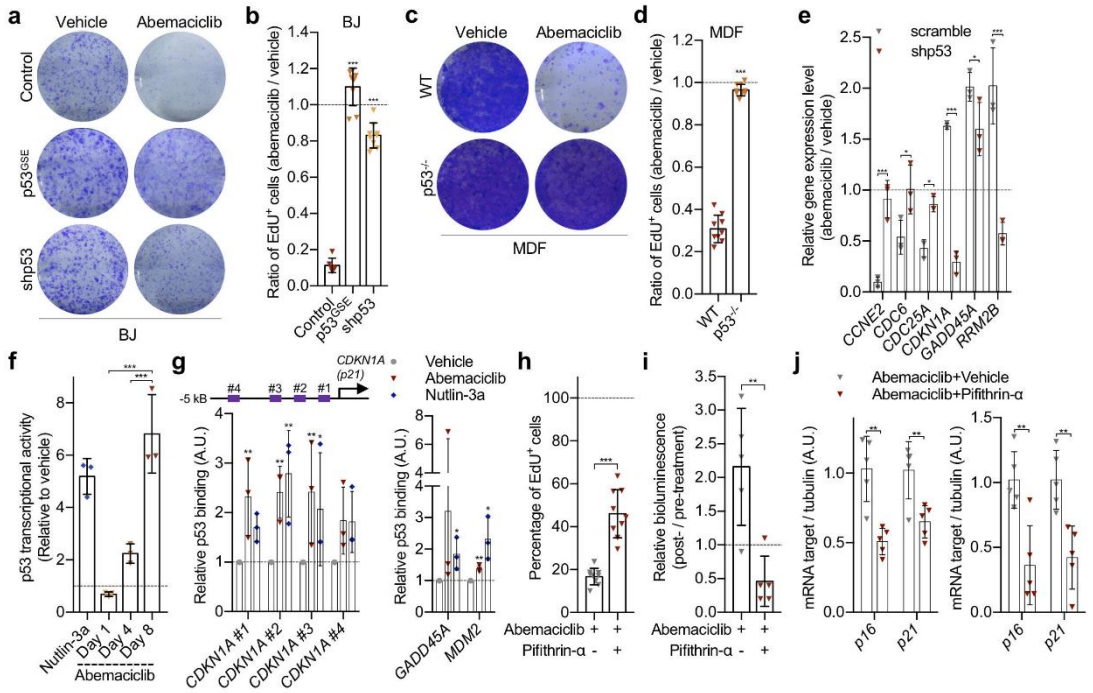

Figure 2. CDK4/6i-induced irreversible growth arrest is dependent on p53. a, 3x10^3 BJ cells of the indicated genotypes were re-plated after vehicle or abemaciclib treatment (1 µM) and stained with 0.2% crystal violet 8 dpt (n=3). **b**, 8 dpt, treated BJ cells were incubated with EdU for 20 hours and stained (n=9). **c**, 3x10^3 mouse dermal fibroblasts (MDFs) of the indicated genotypes were re-plated after vehicle or abemaciclib treatment (4 µM for 8 times 24 hours) and stained with 0.2% crystal violet 8 dpt (n=3). **d**, 8 dpt, treated MDFs were incubated with EdU for 20 hours and stained (n=9). **e**, RNA was isolated from vehicle or abemaciclib (1 µM) treated scramble/shp53 BJ cells and mRNA for the indicated genes quantified by qRT-PCR relative to tubulin (n=3). **f**, BJ cells transduced with a p53 reporter were treated with nutlin-3a (10 µM, positive control) or abemaciclib (1 µM for 1 or 4 or 8 times 24 hours) and luciferase activity measured after treatments at the indicated time points (n=3). **g**, Chromatin was extracted from BJ cells treated with vehicle or abemaciclib (1 µM for 8 times 24 hours) or nutlin-3a (10 µM for 8 times 24 hours) and ChIP assays using an antibody against p53 were performed. qRT-PCR was performed using primers amplifying promoter regions of *CDKN1A*, *GADD45A* and *MDM2* genes containing p53 binding sites. Values indicate fold enrichment relative to the vehicle group (n=3). **h**, 8 dpt, abemaciclib ± pifithrin-α treated BJ cells were incubated with EdU for 20 hours and stained and quantified (n=9). **i**, p16-3MR mice were treated with abemaciclib (50 mg/kg, 7 consecutive days) ± pifithrin-α (2 mg/kg, 7 consecutive days). Values indicate the ratio of post-treatment bioluminescence to pre-treatment (n=5 mice/group). **j**, RNA was isolated from abemaciclib ± pifithrin-α treated livers (left panel) and kidneys (right panel) and mRNA encoding *p16* and *p21* genes was quantified by qRT-PCR and normalized on tubulin (n=5 mice/group). One-way ANOVA, data are means ± s.d. (**b** and **f**). Unpaired two-tailed *t*-test, data are means ± s.d. (**d**, **g**, **h** and **i**). Two-way ANOVA, data are means ± s.d. (**e** and **j**). *p<0.05, **p<0.01, ***p<0.001. dpt, days post treatment.

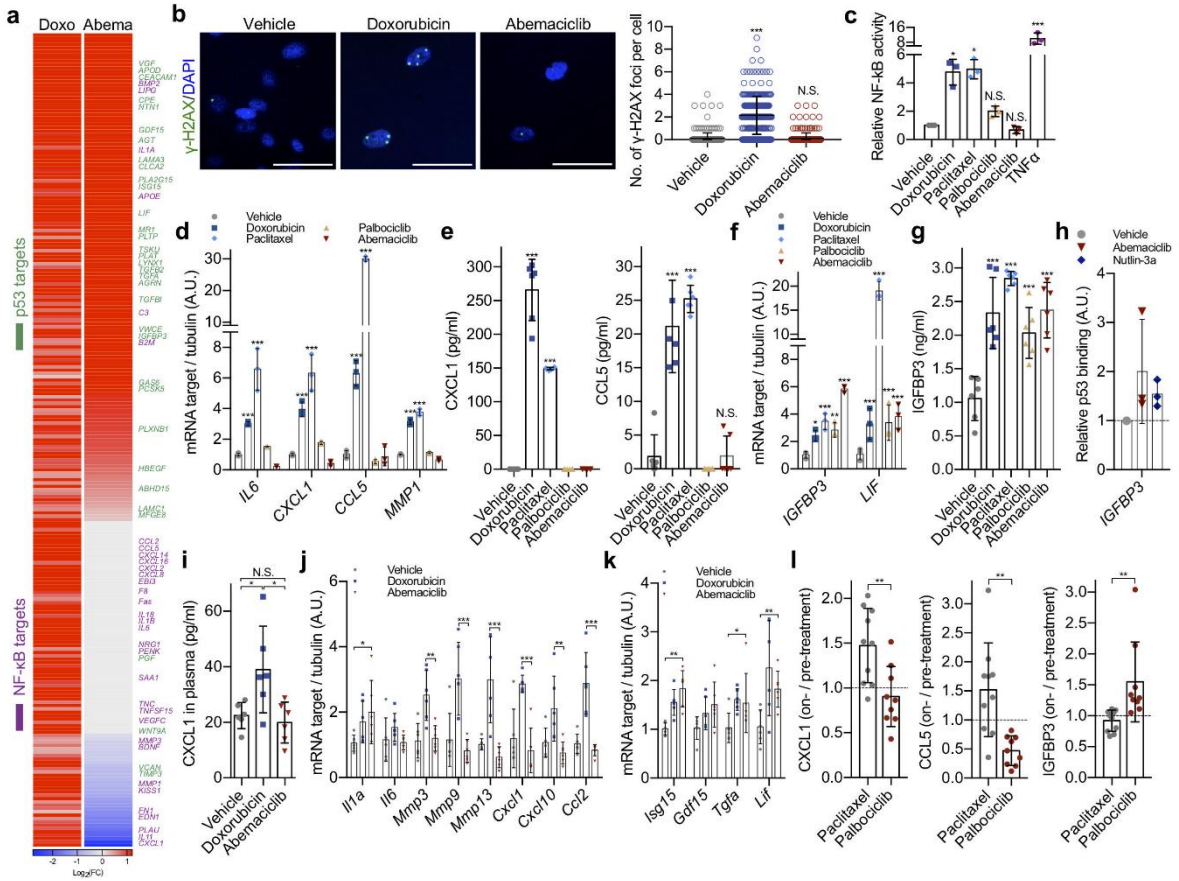

Figure 3. Abemaciclib-induced senescent cells develop only a partial SASP. a, Whole-transcriptome analysis was performed on RNA extracted from human fibroblasts (BJ) 8 dpt with vehicle (water for 8 times 24 hours), doxorubicin (250 nM for 24 hours) or abemaciclib (1 μM for 8 times 24 hours)(n=3). The heatmap represents expression levels of SASP genes for doxorubicin- or abemaciclib-treated groups relative to vehicle-treated group (p-value<0.01). **b**, Human fibroblasts (BJ) were treated with vehicle, doxorubicin or abemaciclib. 8 dpt, cells were stained for γ-H2AX (scale bar, 60 μm) and quantified (vehicle=288 cells, doxorubicin=280 cells, abemaciclib=266 cells from 3 independent experiments). **c**, BJ cells transduced with a NF-κB reporter were treated with vehicle, doxorubicin, paclitaxel (50 nM for 24 hours), palbociclib (1 μM for 8 times 24 hours) or abemaciclib and luciferase activity measured 8 dpt. TNFα treatment was used as positive control (n=3). **d**, 8 dpt, qRT-PCR of indicated genes was performed using indicated treated BJ cells 8 dpt (n=3). **e**, Serum-free conditioned media (CM) was collected from vehicle-, doxorubicin-, paclitaxel-, palbociclib- or abemaciclib-treated BJ cells 8 dpt and expression levels of CXCL1 and CCL5 measured by ELISA (n=6). **f**, 8 dpt, qRT-PCR of indicated genes was performed using BJ cells 8 dpt (n=3). **g**, Expression levels of IGFBP3 measured by ELISA in the CM from (**e**). **h**, Chromatin was extracted from BJ cells treated with vehicle or abemaciclib (1 μM for 8 times 24 hours) or nutlin-3a (10 μM for 8 times 24 hours) and ChIP assays using an antibody against p53 were performed. qRT-PCR was performed using primers amplifying the promoter region of *IGFBP3* containing p53 binding sites. Values indicate fold enrichment relative to the vehicle group (n=3). **i-k**, p16-3MR mice were treated with vehicle (PBS, 7 consecutive days), doxorubicin (5 mg/kg, 3 consecutive days) or abemaciclib (50 mg/kg, 7 consecutive days). n=6 mice/group. 15 dpt, plasma was collected and expression levels of CXCL1 measured by ELISA (**i**), RNA isolated from kidneys and mRNA encoding indicated genes quantified by qRT-PCR (**j** and **k**). **l**, Cell-free plasma was derived from breast cancer patients treated with paclitaxel (n=10) or palbociclib (n=9) and the expression levels of CXCL1, CCL5 and IGFBP3 quantified by ELISA. The values represent the ratio between on-treatment and pre-treatment levels for each patient. One-way ANOVA, data are means ± s.d. (**b**, **c**, **e**, **g** and **i**). Two-way ANOVA, data are means ± s.d. (**d**, **f**, **j** and **k**). Unpaired two-tailed *t*-test, data are means ± s.d. (**l**). *p<0.05, **p<0.01, ***p<0.001, N.S.=not significant. Doxo, doxorubicin. Abema, abemaciclib.

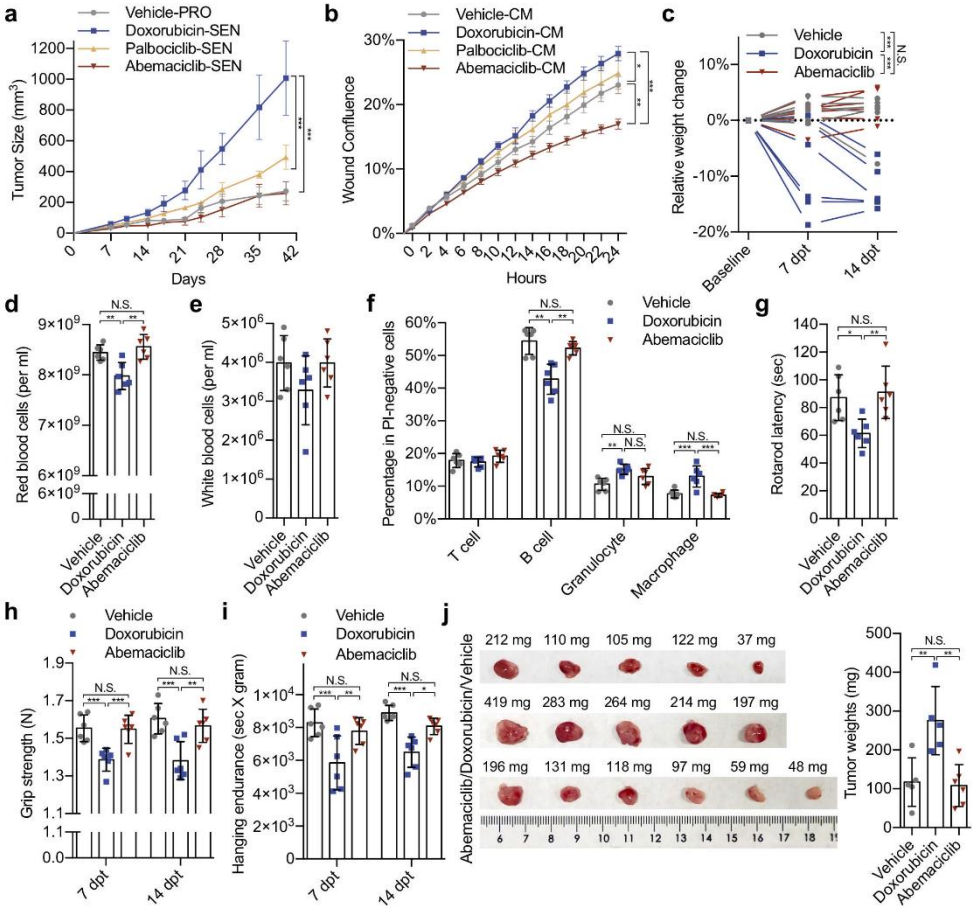

Figure 4. Abemaciclib treatment exerts minimal toxicity. a, Treated BJ cells ($2.5x10^5$) were co-injected with A549 cancer cells (10^6) subcutaneously in *Foxn1*^{Nu} mice and tumor growth measured at the indicated times (n=6 mice/group). **b**, Migration of A549 cells exposed to CM collected from treated BJ cells (8 dpt; n=4) was evaluated using a scratch assay. Imaging and analysis were done using a live imaging system. **c-j**, p16-3MR mice were treated with vehicle (PBS, 7 consecutive days), doxorubicin (5 mg/kg, 3 consecutive days) or abemaciclib (50 mg/kg, 7 consecutive days). n=6 mice/group. Relative weight changes were calculated at 7 dpt and 14 dpt (**c**). Red blood cells (**d**) and white blood cells (**e**) were counted at 15 dpt. Percentage of T cells, B cells, granulocytes and macrophages were determined by flow cytometry analysis (**f**). Physical performance was measured by rotarods assay at 15 dpt (**g**), grip strength meter at 7 dpt and 14 dpt (**h**), and hanging tests were performed at 7 dpt and 14 dpt and normalized to weights (**i**). MMTV-PyMT mouse breast cancer cells were implanted in the mammary fat pad of treated female mice at 14 dpt. 21 days later, the tumors were excised and weighed (left panel, images of the tumors; right panel, tumor weights; n=6 or 7 mice/group) (**j**). Two-way ANOVA, data are means ± s.d. (**a**, **b**, **c**, **f**, **h** and **i**). One-way ANOVA, data are means ± s.d. (**d**, **e**, **g** and **j**). *p<0.05, **p<0.01, ***p<0.001, N.S.=not significant. dpt, days post treatment. PRO, proliferating cells. SEN, senescent cells. CM, conditioned media.

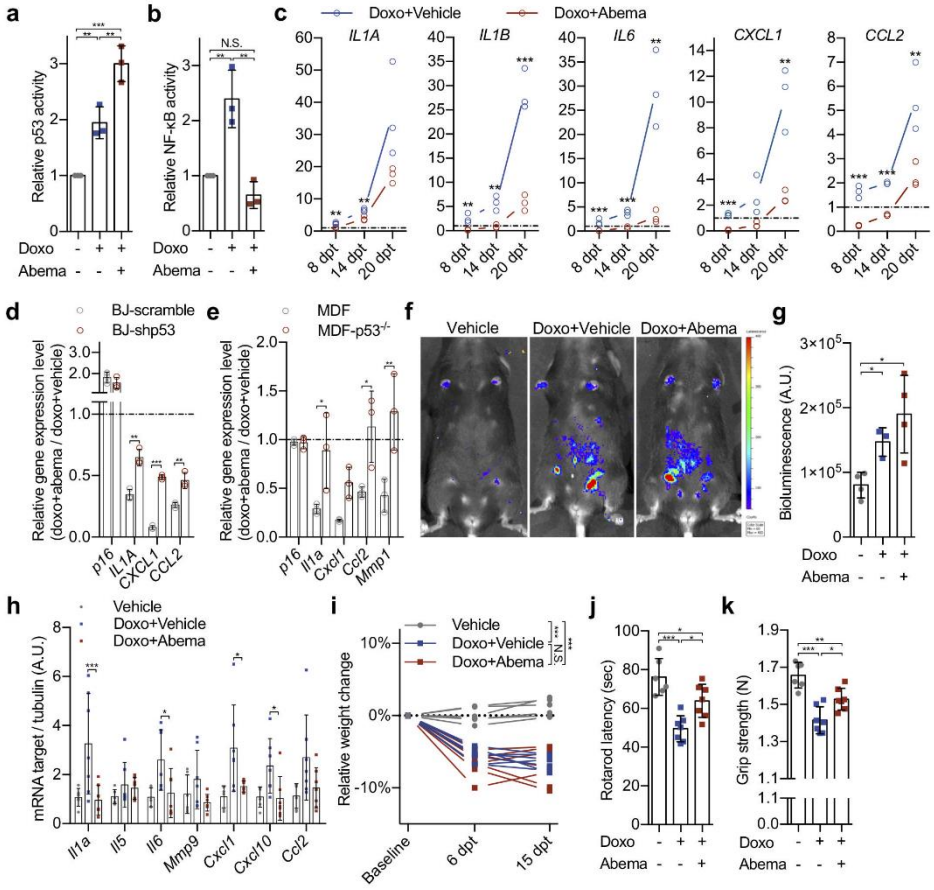

Figure 5. Short-term abemaciclib treatment reduces the SASP of chemotherapy-induced senescence via p53. **a-c**, Cells were treated with vehicle (water) or doxorubicin (doxo; 250 nM for 24 hours) + vehicle or doxo + abemaciclib (abema; 1 μM for 2 times 24 hours at 6 dpt doxo) and all assays were performed at 8 dpt doxo. BJ cells transduced with a p53 reporter (**a**) or NF-κB reporter (**b**) were treated as specified and luciferase activity measured. RNA was extracted from treated BJ cells at the indicated time points and mRNA levels of the indicated genes were quantified by qRT-PCR (**c**) (n=3). **d-e**, RNA was isolated from vehicle or doxo ± abema treated scramble/shp53 BJ cells (**d**) or WT/p53$^{-/-}$ MDFs (4 μM abema) (**e**) at 8 dpt doxo and mRNA levels of the indicated genes quantified by qRT-PCR (n=3). **f-k**, p16-3MR mice were treated with vehicle (3 days with PBS + 6 days of holiday + 3 days with PBS; n=6 mice), doxo+vehicle (3 days with 5 mg/kg doxo + 6 days of holiday + 3 days with PBS; n=7 mice) or doxo+abema (3 days with 5 mg/kg doxo + 6 days of holiday + 3 days with 50 mg/kg abema; n=7 mice). At 16 dpt with doxo, bioluminescence was visualized/quantified by *in vivo* imaging, as shown by representative images (**f**) and quantification (**g**). RNA was isolated from livers and mRNA encoding indicated genes quantified by qRT-PCR (**h**). Relative weight changes were calculated at 6 dpt and 15 dpt doxo (**i**). Physical performance was measured by rotarods assay at 15 dpt doxo (**j**), grip strength meter at 14 dpt doxo (**k**). One-way ANOVA, data are means ± s.d. (**a**, **b**, **g**, **j** and **k**). Two-way ANOVA, data are means ± s.d. (**c**, **d**, **e**, **h** and **i**). *p<0.05, **p<0.01, ***p<0.001, N.S.=not significant. dpt, days post treatment.